 DOI: 10.1002/maco.201307063

Modelling fireside corrosion of thermal sprayed coatings in co-firing of coal/biomass

T. Hussain*, N. J. Simms and J. R. Nicholls

This paper presents a development and evaluation of coating materials for advanced fossil fuel plants and addresses issues related to coal/biomass-derived flue gases. A selection of candidate coatings: 625, NiCr and NiCrAlY were deposited on superheater/reheater materials (T91) using high velocity oxy-fuel (HVOF) spraying. A series of laboratory-based fireside corrosion exposures have been carried out on these coated samples in controlled atmosphere furnaces for 1000 h. The tests were carried out with the "deposit-recoat" test method to generate the exposure conditions; the gaseous environment simulated that anticipated from air-firing 20 wt% cereal co-product (CCP) mixed with a UK coal. The exposures were carried out using various mixtures of Na_2SO_4, K_2SO_4, Fe_2O_3 and kaolinite to produce different deposition fluxes at a test temperature of 650 °C. After the exposures, the samples were examined by environmental scanning electron microscope/energy dispersive X-ray analysis to characterise the damage. Pre- and post-exposure dimensional metrology was used to quantify the metal damage in terms of metal loss distributions. In all three coatings, the deposit targeted at forming undiluted alkali-iron tri-sulphate was found to be the most aggressive, causing the most corrosion damage to all alloys in simulated air-fired combustion gases. A corrosion model was proposed to predict the incubation time at different alkali deposition fluxes. The transition from incubation to propagation was found to be dependent on the chromium content of the alloys. The HVOF NiCr coating, with 46 wt% chromium, was found to be the best performing coating with the longest incubation times in these tests.

1 Introduction

The UK Government has an ambitious target of reducing CO_2 emissions to 80% of their 1990 levels by 2050 and generating 20% of the energy from renewable sources by 2020 [1, 2]. To meet these targets renewable fuel such as biomass will play a significant role. Co-firing biomass with coal is a near term option to reduce CO_2 emissions from the utility boilers and to increase the energy output from renewable sources [3, 4]. At present, conventional fossil fuel-fired power plants are believed to be significant contributors to the enhanced greenhouse effect/global warming [1, 5]. Co-firing low levels of biomass in conventional pulverised coal-fired power plants has proved to be a successful way to introduce carbon neutral biomass fuels into the electricity generation market. Biomass is a major contributor to renewable energy production, accounting for approximately 70% of world-wide renewable energy production [6]. In addition, increasing the efficiency of boilers by increasing the operating steam temperatures (and pressures) is an attractive option for power plant operators to reduce the greenhouse gas production and to meet increasingly stringent legislations. However, the superheaters/reheaters in such system may encounter very aggressive fireside corrosion at the operating temperatures required to improve plant efficiency and make CO_2 capture systems viable. The use of biomass and higher operating temperature are dependent on the development of high temperature corrosion resistance alloys.

Fireside corrosion is defined as the loss of heat exchanger metal due to chemical reactions with the combustion gases and deposits at high temperatures [7–9]. Fireside corrosion is the single most reason for tube failures for pulverised fuel-fired power plants [8–11]. These failures are difficult to repair and result in unscheduled plant down time. Fireside corrosion in pulverised coal-fired power plants has been studied widely and it has shown that molten alkali-iron tri-sulphates can form in the deposits on heat exchanger surfaces and are very aggressive in

T. Hussain, N. J. Simms, J. R. Nicholls
Centre for Energy and Resource Technology, Cranfield University, Bedfordshire, MK43 0AL (UK)
E-mail: t.hussain@cranfield.ac.uk

nature [8, 11]. When biomass is co-fired with coal the combustion gases and deposits do not remain the same. The environment is expected to be chemically more aggressive, with particles leading to erosion or deposition, while chemically corrosive species depositing on the heat exchanger surface leading to fireside corrosion. The rates of corrosion will depend (amongst other factors) on the rate of deposition, deposit composition, the metal temperature and the composition of surrounding gas environment. The deposition of alkali bearing salts and the onset of fireside corrosion is a serious and a life-limiting problem. This paper addresses this issue, namely the modelling and predicting of fireside corrosion of superheaters/reheaters in pulverised fuel power plants.

High corrosion resistant Ni-based alloys can provide suitable protection from fireside corrosion but Ni-based alloys are 10 times more expensive than conventional ferritic steels. It is considered that the development and use of effective corrosion resistance coatings will enable power plants to operate at higher steam temperatures (and pressures), hence increasing efficiency, and also utilise lower grades of fuel. Thermally sprayed coatings can be applied to both new build power plants and retrofit applications. Thermally sprayed coatings on low-cost substrate materials (e.g. steels with sufficient creep strength) can provide a cost-effective solution in this aggressive environment [12]. Among the thermal spray techniques, the high velocity oxy-fuel (HVOF) is widely used to produce corrosion resistant coatings with low porosity, high density and excellent adhesive strength [13]. In HVOF process oxygen and a fuel (usually a gas) are mixed and burnt in the combustion chamber of a spray gun. The high gas pressures and temperatures are used to heat and accelerate the powder particles toward a substrate [14]. The powder particle temperatures are relatively low and particle velocities are relatively high in comparison with other thermal spraying processes [15]. HVOF process can produce Ni alloy coatings for corrosion resistance applications, where dense, microstructurally homogeneous coatings are essential.

This paper presents the results of an investigation into the fireside corrosion performance of three thermally sprayed coating: 625, NiCr and NiCrAlY on T91 boiler steel in simulated air-fired combustion gases (1300 vppm SO_2 and 400 vppm HCl) at 650 °C for 1000 h. The tests were carried out with the ''deposit-recoat'' test method that has been established for high temperature corrosion. The exposures were carried out using five different mixtures of Na_2SO_4, K_2SO_4, Fe_2O_3 and kaolinite to produce different deposition fluxes. Section loss data have been measured and analysed statistically, from which a fireside corrosion model of thermally sprayed coatings for potential use in superheaters/reheaters in a pulverised fuel power plant has been developed.

Table 2. Nominal gas composition used in fireside corrosion tests

	N_2 (vol%)	O_2 (vol%)	CO_2 (vol%)	H_2O (vol%)	SO_2 (vppm)	HCl (vppm)
Air-firing	73.8	4	14	8	1300	400

2 Experimental methods

2.1 Materials

In this study, three thermal sprayed coatings: alloy 625, NiCr and NiCrAlY were sprayed onto a ferritic steel T91 (0.07–0.14 C, 0.2–0.5 Si, 0.3–0.6 Mn, 8.0–9.5 Cr, 0.85–1.05 Mo, 0.18–0.25 V, 0.03–0.07 N, 0.06–0.1 Nb, $\leq$0.4 Ni wt%) by Sulzer Metco, Inc. (USA) with commercially available powders from Sulzer Metco, Inc. Nominal compositions of the coatings are given in Table 1. All three coatings have been traditionally applied in high temperature corrosion resistance applications. NiCr is a high chromium content (46 wt%) alloy, alloy 625 has 21 wt% Cr with 9 wt% Mo and 3.6 wt% Nb + Ta and NiCrAlY contains 9 wt% Al with 22 wt% Cr. All three coatings were applied on a 38 mm diameter boiler tube (T91) using HVOF spraying using propylene as the liquid fuel. T91 was used as a substrate material to represent candidate materials for heat exchangers (supeheater/reheaters) in advanced pulverised fuel power plants. The coated tubes were cut and machined into tube segments with dimensions of ~15 mm chord, 15 mm long and 5 mm wall thickness.

2.2 Exposure conditions

The exposure conditions were determined following a detailed investigation of the gaseous environments and deposit conditions that could be found around superheaters/reheaters in conventional pulverised coal-fired UK plants using various biomass-coal fuel combinations [8, 10, 16, 17]. The gaseous conditions for the fireside tests were based on co-firing 80:20 wt% of a typical UK coal (Daw Mill) with cereal co-product (CCP). The compositions of these fuels are available in [18]. The combusted gas compositions produced by these fuels have been calculated from the fuel compositions, using models that have been validated through pilot and plant scale operations. These gas compositions have been simplified to their key active components for the purposes of corrosion testing in superheaters/reheaters environments. The nominal composition of the gas is given in Table 2. The coatings were tested at 650 °C in the simulated air-fired combustion gas for 1000 h.

Five deposit compositions were selected for application in this test programme (Table 3). D1 is a widely used standard deposit for screening tests in fireside corrosion as it represents

Table 1. Nominal composition (wt%) of the coatings used in fireside corrosion exposures

	Al	C	Co	Cr	Cu	Fe	Mo	Nb + Ta	Si	Y	N	O	Ni
Alloy 625	0.2		0.1	21.3	0.18	0.1	8.9	3.58	0.13		0.03		Bal.
NiCr		0.1		46.0		1.1			2.1			0.03	Bal.
NiCrAlY	9.9			22.0						0.9		0.02	Bal.

Table 3. Deposit compositions (mol%) used in fireside corrosion tests

Deposits	Kaolinite[a]	Na_2SO_4	K_2SO_4	Fe_2O_3
100% Alkali (D1)	0	37.5	37.5	25
80% Alkali (D2)	20	30	30	20
40% Alkali (D3)	40	22.5	22.5	15
60% Alkali (D4)	60	15	15	10
20% Alkali (D5)	80	7.5	7.5	5

[a] $Al_2O_3{\cdot}2SiO_2{\cdot}2H_2O$.

a composition of alkali-iron tri-sulphate that has been identified as being the principle cause of fireside corrosion on superheaters/reheaters in pulverised coal-fired stations [7, 8, 11, 17, 19, 20]. This deposit is referred to as 100% alkali in this paper, as it represents a mixture which can produce 100% alkali-iron tri-sulphates. The alkali-iron tri-sulphate compositions from D1 were diluted with 20, 40, 60, 80 (mol)% kaolinite ($Al_2O_3{\cdot}2SiO_2{\cdot}2H_2O$) to represent the clay minerals usually found in coals. These mixed deposits represent that formed by mixed deposition routes (particle and vapour deposition) on superheater/reheater surfaces [5, 8, 9, 11, 16, 19]. These deposits are referred to according to the amount of alkali-iron tri-sulphate they produce (i.e. deposit with no kaolinite is referred to as 100% alkali and deposit with 80% kaolinite is referred to as 20% alkali). The deposits were mixed with isopropanol (IPA) to form thick slurries for painting onto the specimens.

2.3 Experimental setup

The fireside corrosion exposures were carried out in an alumina-lined vertical controlled-atmosphere furnace using simulated air-fired combustion gas. The furnace holds 24 test pieces at one time in individual alumina crucibles in the hot zone. Pre-mixed gases were supplied to the controlled-atmosphere furnace through mass flows controllers to achieve the desired gas composition. The schematic diagram of the furnace set-up to simulate air-firing conditions is shown in Fig. 1. In the experimental set-up, the gas containing (CO_2, O_2, N_2) was passed through a de-ionised water bubbler which was kept at 40 °C in a water bath to add the required amount of moisture to the gas stream before mixing with the corrosive species (HCl, SO_2). The exhaust gases from the furnace passed through an initially empty bottle to trap the condensate and then through a scrubber solution (NaOH) before finally being released into the atmosphere.

Each test was run for 1000 h using the widely accepted "deposit-recoat" method [17, 21–23]. The samples were cleaned before exposure using a degreaser (volasil) followed by IPA in an ultrasonic bath for 20 min. The cleaned samples were painted using a paint brush to apply a deposit loading of ~20 mg/cm^2. The tests were cycled every 200 h and repainted with deposits to replenish any salts, resulting in a deposition flux of ~100 μm/cm^2/h. The samples were weighted every 200 h with and without crucibles as well as before and after applying the deposits.

2.4 Pre- and post-exposure measurements

Following exposure the samples were vacuum mounted using a low shrinkage cold mounting resin filled with ballotini (to further reduce shrinkage) in a specially designed jig. The mounted samples were then cross-sectioned, ground and polished to 1 μm diamond grit finish using non-aqueous lubricants. Environmental scanning electron microscope (ESEM) was used to investigate the scale layer thicknesses and microstructures on the polished cross-sections. Energy dispersive X-ray (EDX) spectroscopy was used to identify the composition of the scales/deposits on the cross-sections. To identify the elemental distribution of key components across the scale/metal interfaces EDX mapping was used.

The dimensions of each of the samples were measured before and after the exposure. The dimensional metrology of the

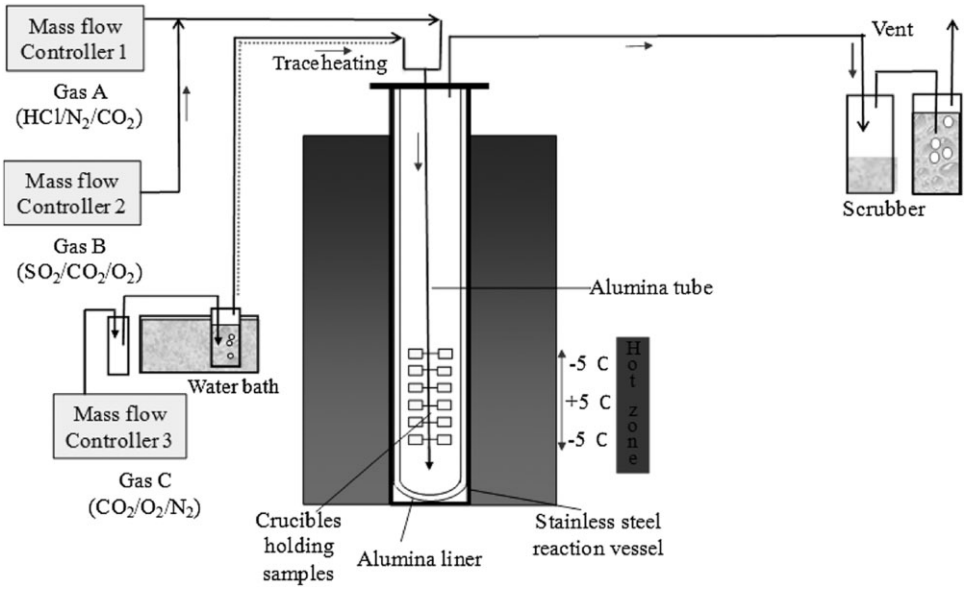

Figure 1. Schematic diagram of a controlled atmosphere furnace setup for fireside corrosion in simulated air-firing combustion gases

samples before and after exposure in the fireside corrosion tests is a key element of this research. All samples were measured using a digital micrometer (with resolution of 1 μm) prior to their exposure. Post-exposure metrology on sample cross-sections was carried out using an image analyser connected to an optical microscope with a motorised x–y co-ordinate table, to determine the remaining metal thickness and any internal damage. The measured co-ordinates from the post-exposure image analysis were transferred into spreadsheets and compared with the pre-exposure micrometer measurements to determine a metal loss data distribution for each sample. These distributions were further processed to generate cumulative probability curves. A detailed description of the method is available in previously published papers [18, 24]. This measurement method was performed in accordance with the draft standard methods for high temperature corrosion assessments [21–23].

3 Results

3.1 Mass change data

Mass change data are the most conventional and frequently reported method of observing metal oxidation and corrosion at high temperatures [25, 26]. Figure 2 shows the specific mass change data for individual samples of alloy 625, NiCr and NiCrAlY covered with five deposits (100, 80, 60, 40 and 20%) in simulated air-fired combustion gases. Figure 2 shows an approximately linear kinetics of the fireside corrosion for all three coatings covered in various deposits. In such mass change plots, the increase in mass change corresponds to oxidation/sulphidation of the sample in the simulated air-fired combustion gases and the decrease in mass change corresponds to spallation/evaporation. Rapid mass gain was observed in all three coatings when 100% alkali deposits were applied, even within first 200 h cycle. With the rest of the deposits (e.g. 80–20% alkali) similar mass gain were observed for all three coatings. Following 200 h of exposure, the samples with higher quantity of alkali showed higher mass gain in a linear fashion. When all three types of coatings were covered with 20 and 40% alkali deposits similar specific net mass gain up to 600 h were observed, after which the sample covered with 40% alkali resulted in a higher mass gain than that of the sample covered with 20% alkali.

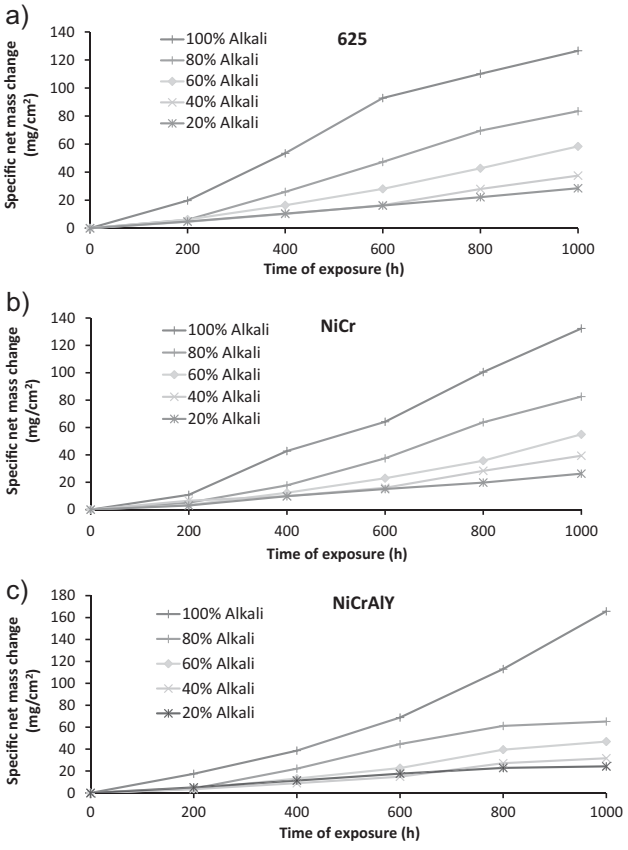

Figure 2. Mass change data for coatings: (a) 625, (b) NiCr and (c) NiCrAlY covered with deposits containing (100, 80, 60, 40 and 20) % alkali in simulated air-fired combustion gases

The mass change of each alloy is sensitive to the quantity of alkali present in the deposits, with mass gain/corrosion damage increasing with increasing alkali percentages in the deposits. Under the most aggressive conditions of 100% alkali deposit, the coating NiCrAlY showed the highest mass gain out of all three candidate coatings. Conventional parabolic kinetics of high chromium alloys were not observed in any of the samples. Although mass change data provide valuable information about the kinetics of the high temperature oxidation/corrosion mechanisms, there are drawbacks to using mass change data, such as spalling of oxides/corrosion products/deposits during the course of exposure or through thermal cycling and formation of volatile species [21, 23]. Hence, dimensional metrology was performed to investigate the damage of the samples following exposures in the fireside corrosion tests.

3.2 Measurements of metal damage (dimensional metrology)

Dimensional metrology is the best measurement method available for corrosion performance of the different alloys, as the method produces a distribution of metal damage data for each exposed sample. The results are plotted as change in metal thickness *versus* cumulative probability according to draft standards for high temperature corrosion measurements [21, 22]. Cross-sections from each test environment were measured using an image analysis system to provide datasets of ~20 metal loss measurements. These datasets for each sample are then ordered to allow the extent of attack to be determined and presented as probability plots [24, 27].

Figure 3 illustrates such plots for alloy 625, NiCr and NiCrAlY after 1000 h exposure at 650 °C in simulated air-fired combustion gases with five different deposits. The data for 625 (Fig. 3a) demonstrate that measured metal losses with 20 and 40% alkali are generally less than 10 μm (close to the accuracy of the measurement techniques, which is ±5 μm). Both, the samples are considered still to be in their incubation periods, where the damage to the protective scale can be repaired by the elements in the underlying material [28]. However, with increasing the concentration of active species, which take part in the corrosion reactions, the damage to the alloy had increased.

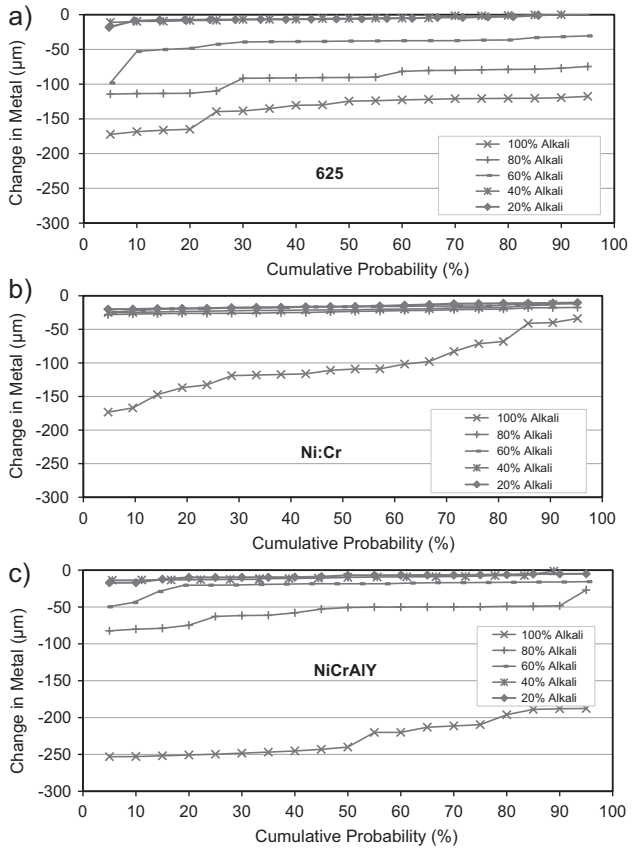

Figure 3. Change in metal thickness *versus* cumulative probability showing the behaviour of coatings: (a) 625, (b) NiCr and (c) NiCrAlY covered with deposits containing (100, 80, 60, 40 and 20) % alkali in simulated air-fired combustion gases

For this coating, a shift from incubation to the propagation occurred at 60% alkali deposit. Median metal loss (at 50% probability) of the 625 sample covered with 60% alkali deposits was 38 μm, the sample covered with 80% alkali was 90 μm and the sample covered with 100% alkali was 125 μm. The samples covered with all three deposits are considered to be in propagation stages as all the data points recorded from these samples are significantly greater than zero. The distribution of change in metal of 625 covered with 100% alkali shows that the 25% of the sample have an increased penetration up to 170 μm. Similarly, the distribution of 625 alloy covered with 80% alkali deposit shows that 25% of the sample surface suffered an increased penetration up to 115 μm. Regions of the cumulative probability plots that are effectively flat correspond to an even distribution of change in metal.

Figure 3b illustrates a cumulative probability plot for NiCr coating covered with five different levels of alkali deposits following exposure at 650 °C for 1000 h in simulated air-fired combustion gases. Cumulative probability plots of 20, 40, 60 and 80% alkali deposits showed no significant differences in change in metal values (all the samples were in incubation where changing the levels of alkali content in the deposits did not show any measurable distinction in metal loss values). Median metal loss values in 20–80% alkali deposits were below 15 μm and the cumulative probability plots were approximately straight lines indicating an even distribution. However, NiCr coatings covered in 100% alkali deposits showed a significant change in metal that is all the measurements on the sample were higher than zero. The steep sections of the plot show that the sample has suffered damage of various depths. The plot illustrates that 80% of the surface of the sample suffered a loss of metal greater than 70 μm. Thus, the whole sample surface was in propagation stage when it was covered in 100% alkali deposit.

The plots of NiCrAlY alloy (Fig. 3c) demonstrate that the coatings covered in 20 and 40% alkali deposits showed metal losses less than 7 μm (close to the accuracy of the measurements). The whole of these sample surfaces are considered to still be in the incubation stage. The change in metal distribution of the alloy covered in 60% alkali showed a small increase in median metal loss (18 μm), with 15% of the sample with more than 29 μm metal loss. The different areas of the sample moved into the propagation stage from the incubation stage at different rates. The change in metal distribution for NiCrAlY coating covered with 60% alkali deposits shows a median metal loss of 50 μm and 50% of the sample surface suffered corrosion attack of more than 50 μm. The sample was well into the propagation stage. It is apparent that when NiCrAlY was covered with 100% alkali deposit in the simulated air-fired combustion gases catastrophic failure of the coating occurred; 50% of the sample surface suffered a corrosion damage of >250 μm (as-sprayed thickness of the coating was ~250 μm) leaving 50% of the surface without any coating. This implies that above a certain percentage of alkali in the deposits (or flux) rapid attack can occur on NiCrAlY coatings.

3.3 Microstructural investigations

Following the preparation of cross-sections for dimensional metrology, all exposed samples were examined in an ESEM in environmental scanning mode, along with as-sprayed coatings. Figure 4 illustrates some of the morphologies observed in the BSE mode, as a function of alkali content in the deposits.

Cross-sectioned of as-sprayed alloy 625 sample shows a pore-free micro-structure of ~250 μm thick coating on T91 substrate. The areas of darker contrast at the coating-substrate interface are alumina grit (identified by EDX analysis) from the surface preparation step before spraying. Following exposure in simulated air-fired combustion gases for 1000 h, alloy 625 coating covered with 100% alkali deposit showed aggressive corrosion attack similar to broad front type II hot corrosion attack. The darker contrast layers on top of the coatings were identified as deposit/corrosion product layers. EDX mapping (not shown here) showed sulphur rich region on the top of the coatings. This sulphidation indicates that the sample's initial protective oxide layer had been damaged and that corrosion was in the propagation stage. In contrast, the sample which was exposed with 20% alkali deposits showed little corrosion attack and the deposits were mostly un-reacted. A thin oxide layer rich in chromium was present across the entire sample surface indicating that the sample was still in incubation.

The as-spayed microstructure of NiCr and NiCrAlY coatings are also shown in Fig. 4. Typical thickness of both coatings was

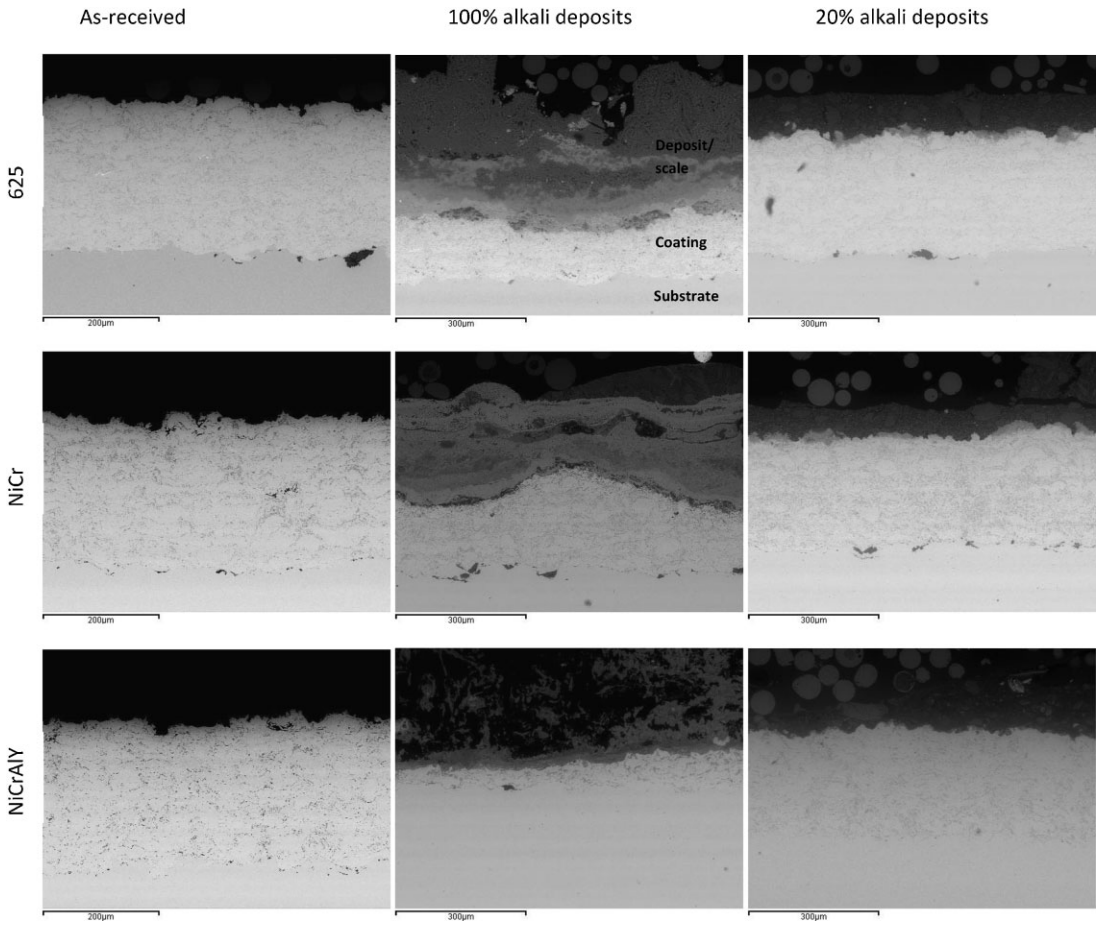

Figure 4. BSE images of cross-section of the coatings 625, NiCr and NiCrAlY on T91 substrate in as-received, covered with deposits containing 100 and 20 % alkali in simulated air-fired combustion gases after 1000 h

~250 µm. Similar to alloy 625, NiCr coating covered in 100% alkali deposits showed significant loss of coating thickness. A thick band of sulphur was detected on top of the coatings in the EDX map which confirms sulphidation attack. A thick band of corrosion products (deposits/scales) can be seen on the top of the coating in the BSE image. The microstructure of NiCrAlY coating covered in 100% alkali deposits showed only 20–30 µm thick coating left on the substrate. As it was found from the dimensional metrology studies, 50% of the surface of this sample did not have any coating left and the remaining surface only had a thin layer of coating. An elaborate network of sulphur was present in the deposit/scale, as seen in EDX maps. In contrast, both NiCr and NiCrAlY samples covered in 20% alkali deposits showed no attack of the coating. The deposits were largely un-reacted on these samples.

4 Discussion

4.1 Modelling the incubation-propagation rates

From the foregoing results section it is evident that for the coatings studied in this paper (625, NiCr, NiCrAlY) the transition from incubation to catastrophic propagation occurs at various levels (or fluxes) of active elements (alkali content) in the deposits. The ordered metal loss data allow the sensitivity of fireside corrosion damage at a particular probability level to be assessed as influenced by various environmental parameters that is salt chemistry. The changes in the metal loss measured in this study can be used to develop models for the rate of growth of fireside corrosion as a function of salt flux.

It is evident from the metal loss data that the observed corrosion damage is a complex interaction between alloy chemistry and salt chemistry (in simulated combustion gases at high temperatures). This is due to the complexity of the alloy and gas induced acid fluxing reactions and how these fluxing reactions interact with salt supply. The 100% alkali deposit is a widely used screening deposit in fireside corrosion tests as it represents a composition of alkali-iron tri-sulphate that has been identified by several researchers as being the principle reason for superheater/reheater corrosion in pulverised coal-fired power plants [8, 11, 17, 19, 20]. The mass change data of the alloys (Fig. 2) covered with 100% alkali deposits showed rapid mass gain, even after 200 h, indicating an aggressive corrosion attack. The mechanisms of corrosion in all five deposit compositions can be considered similar as the active elements are the same in all deposits, albeit at different dilutions. Addition of kaolinite to the deposits should not change the mechanisms of corrosion as

kaolinite remains unreacted in these exposure temperatures in this environment.

Figure 5 illustrates the incubation-propagation type plots for 625, NiCr and NiCrAlY coatings. For each type of deposit median metal loss values from Fig. 3 were taken. Alloy 625 covered with 20 and 40% alkali deposits were still in incubation stage as the median metal losses were very small (near the accuracy of the measurement technique). The sample covered in 100% alkali deposits was in its propagation stage during the whole period of the exposure (as can be seen from the mass change data). If the same corrosion propagation mechanisms are found in the rest of the samples (i.e. samples covered with 60 and 80% alkali deposits) then straight lines parallel to the 100% alkali deposit can be drawn from their corresponding median metal loss values which intersect the incubation line at 730 and 280 h, respectively. It is found that the alloy 625 sample covered in 60% alkali deposit had an incubation period of ~730 h, after which the sample entered into the propagation stage. Similarly, alloy 625 covered in 80% alkali deposit was in its incubation stage till ~280 h before entering into the propagation stage.

Similar damage *versus* exposure time plots can be drawn for NiCr coatings covered in 100, 80, 60, 40 and 20% alkali deposits. It is interesting to notice that all the samples covered in deposits, except 100% alkali deposits, showed very little corrosion damage, hence the incubation times for the onset of fireside corrosion for those samples were more than ~900 h. NiCr coating was very resilient to the increase in alkali percentages in the deposits and only showed aggressive corrosion attack when 100% alkali deposit was used.

Figure 5c illustrates the incubation-propagation plots for NiCrAlY coatings for all five different deposits. The gradient for corrosion damage of the NiCrAlY sample covered in 100% alkali deposit was steeper compared to NiCr and alloy 625 coatings, as the median metal loss was higher compared to the other two coatings. Alloy 625 and NiCrAlY had similar amount of Cr in the coatings but alloy 625 had Mo, Nb and Ta, which contributed to produce a more adherent protective oxide scale. Although, NiCrAlY contained 9 wt% Al, the temperature was not sufficient to produce a protective alumina layer at 650 °C. The samples covered with 20 and 40% alkali deposits were in incubation stages until 1000 h. The sample covered in 60% alkali deposit showed a small increase in metal loss value and had an incubation period of ~950 h. However, the sample covered in 80% alkali deposit was in incubation up to ~820 h. It is interesting to notice that NiCrAlY coating has longer incubation times compared to alloy 625 samples; however, when the propagation commences it progresses more rapidly in NiCrAlY.

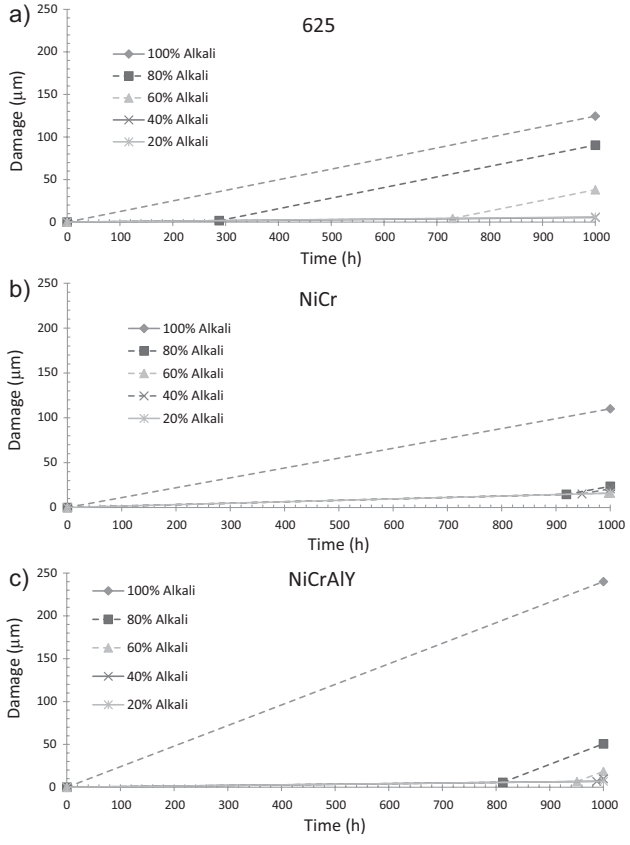

Figure 5. Damage *versus* exposure time showing the incubation to propagation type behaviour of coatings: (a) 625, (b) NiCr and (c) NiCrAlY covered with deposits containing (100, 80, 60, 40 and 20) % alkali in simulated air-fired combustion gases

4.2 Prediction of incubation time

The incubation times derived from Fig. 5 for various alloys and deposit compositions can be used to model incubation times for alloys at different alkali fluxes. The samples were painted to apply a deposit loading of ~20 mg/cm^2 and the test was cycled every 200 h and repainted with deposits to replenish any salts according to "deposit-recoat" draft test methodology, giving a deposition flux of 100 μm/cm^2/h. Thus, all the deposits with five levels of alkali concentration can be converted to deposition flux (μm/ cm^2/h). Figure 6 illustrates incubation time *versus* deposition flux plots for alloy 625 and NiCrAlY coatings. It was not possible to produce such plots with the incubation times from NiCr coating as most of the samples, except the sample covered in 100% alkali deposit, was in incubation mode during the test duration of 1000 h.

In Fig. 6a, first three data points were used to draw a straight line which intersects the Y-axis at 1800 h which means alloy 625 with a low (near zero) deposition flux has an incubation time of at least 1800 h. The samples with 20 and 40 μm/cm^2/h deposition fluxes were still in incubation up to 1000 h so their accurate position on the plot cannot be determined, but it can be anticipated that the incubation times will be higher. Similarly, Fig. 6b shows the incubation time *versus* fluxes for NiCrAlY coatings. Incubation times at 100, 80 and 60 μm/cm^2/h were used to draw a straight line, which shows that at low (near zero) flux incubation time for NiCrAlY is at least 2500 h. Although, generally the incubation time of NiCrAlY is higher than alloy 625, when the corrosion moves into the propagation mode it accelerates very rapidly.

These types of plots provide valuable information for coating/boiler manufacturers and operators who can then design a corrosion resistant system with known deposition flux and predict after how long the alloy will enter the propagation stage.

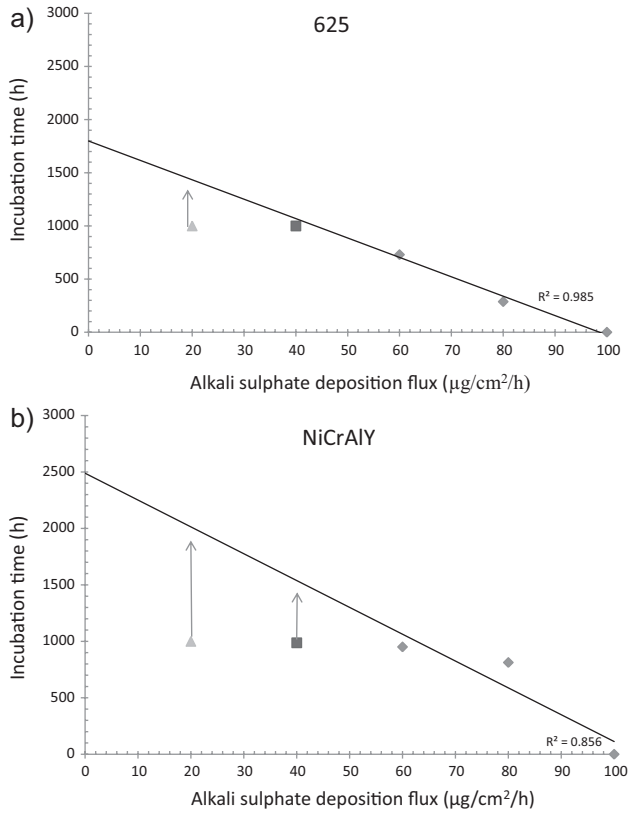

Figure 6. Incubation time *versus* deposits flux for coatings (a) 625 and (b) NiCrAlY in simulated air-fired combustion gases

Work is in progress to develop this model further. Currently, the model predicts incubation time assuming the rate of propagation is same for the deposits with same active elements on the same alloy. Further test work is in progress to validate the transition points (from incubation to propagation) in the model.

5 Conclusions

This paper reports the results of a series of laboratory tests carried out to systematically investigate the role of alkali-iron tri-sulphate deposition flux on fireside corrosion of three nickel-based thermally sprayed coatings: alloy 625, NiCr and NiCrAlY on a boiler steel (T91). The environments were selected to simulate the conditions anticipated around superheaters/reheaters in pulverised fuel boiler firing a mixture of UK coal with CCP. The exposures were carried out at 650 °C for 1000 h using well-established deposit-recoat method. Dimensional metrology has been used as the primary route for quantifying this damage, along with traditional mass change data.

Deposit D1, simulating undiluted alkali-iron tri-sulphate, was found to be the most aggressive deposit causing more corrosion damage to all alloys in simulated air-fired combustion gases. The transition from the incubation phase to the propagation phase is confirmed to be dependent on the chromium content of the alloys. NiCr coating with 46 wt% chromium can have incubation times up to ~900 h for an alkali-iron tri-sulphate deposition flux of 80 μg/cm^2/h at 650 °C. Whereas, alloy 625, with 21 wt% chromium content enters the propagation phase within ~280 h of testing at 650 °C for a deposition flux of 80 μg/cm^2/h. In these tests, only NiCr coatings covered in 100% alkali deposits were in propagation stages, whereas the rest of the NiCr samples were in incubation phase. The incubation times for NiCrAlY were higher than those of alloy 625; however, when the corrosion of NiCrAlY moved into the propagation mode it accelerated rapidly.

A corrosion model has been derived to predict the incubation times in fireside corrosion in presence of complex alkali-iron tri-sulphate deposits expected in the superheater/reheater environment in pulverised fuel power plants, when co-fired on a specific coal and biomass mix. Such models can be very useful for coating/boiler manufacturers and operators to predict incubation time at various deposition fluxes.

Acknowledgements: The authors acknowledge the support from ASPECT project, which is a Technology Strategy Board project, and specifically to the following companies; Doosan Babcock, E.ON, National Physical Laboratory, Sulzer Metco, Monitor Coatings, and RWE npower, for their valuable contributions to the project.

6 References

[1] J. Skea, P. Ekins, Min: UKERC energy 2050 project; S3097: 302009. **2009**.
[2] DTI. DTI Report URN 07/950, **2007**. p. 1.
[3] A. L. Robinson, H. Junker, L. L. Baxter, *Energy Fuels* **2002**, *16*, 343.
[4] D. A. Tillman, *Biomass Bioenergy* **2000**, *19*, 365.
[5] B. Bordenet, *Mater. Corros.* **2008**, *59*, 361.
[6] A. A. Khan, W. de Jong, P. J. Jansens, H. Spliethoff, *Fuel Process. Technol.* **2009**, *90*, 21.
[7] N. J. Simms, in: J. E. Oakey, (Ed.), *Power Plant Life Management and Performance Improvement*, Woodhead Publishing, Cambridge **2011**, p. 145.
[8] N. J. Simms, P. J. Kilgallon, J. E. Oakey, *Energy Mater. Mater. Sci. Eng. Energy Syst.* **2007**, *2*, 154.
[9] N. J. Simms, P. J. Kilgallon, J. E. Oakley, *Mater. High Temp.* **2007**, *24*, 333.
[10] T. Hussain, A. U. Syed, N. J. Simms, Oxid. Met. **2013**, DOI: 10.1007/s11085-9394-y
[11] J. Stringer, I. G. Wright, *Oxid. Met.* **1995**, *44*, 265.
[12] S. Paul, M. Harvey, *J. Therm. Spray Technol.* **2013**, *22*, 316.
[13] M. Magnani, P. Suegama, N. Espallargas, C. Fugivara, S. Dosta, J. Guilemany, A. Benedetti, *J. Therm. Spray Technol.* **2009**, *18*, 353.
[14] H. Edris, D. McCartney, A. J. Sturgeon, *J. Mater. Sci.* **1997**, *32*, 863.
[15] M. Oksa, T. Varis, T. Suhonen, M. Jokipii, in: *Thermal Spray 2012: Proceedings of the International Thermal Spray Conference*, ASM International, Houston, TX **2012**.
[16] N. J. Simms, A. T. Fry, in: *Materials for Advanced Power Engineering Proc.*, eds. J. Lecomte-Beckers, M. Carton Forschungszentrum, Jülich **2010**.
[17] T. Hussain, T. Dudziak, N. J. Simms, J. R. Nicholls, *J. Therm. Spray Technol.* **2013**, *22*, 1.
[18] A. U. Syed, N. J. Simms, J. E. Oakey, *Fuel* **2012**, *101*, 62.

[19] E. Raask, *Mineral Impurities in Coal Combustion*, Hemisphere Publishing Corporation, Washington **1985**.
[20] K. Natesan, A. Purohit, D. L. Rink, in: US Department of Energy Fossil Energy Conference **2003**.
[21] Draft Code of Practice for Discontinuous Corrosion Testing in High Temperature Gaseous Atmospheres, in: *EC project SMT3-CT95-2001, TESTCORR. UK: ERA Technology* **2000**.
[22] Corrosion of Metals and Alloys-Methods for Metallographic Examination of Samples After Exposure to High Temperature Corrosive Environments; in: *Draft ISO Standard. ISO/TC 156 NWI 509*, **2005/2006**.
[23] S. R. J. Saunders, in: H. J. Grabke, D. B. Meadowcroft, (Eds.), *Guidelines for Methods of Testing and Research in High Temperature Corrosion*, The Institute of Metals, London **1995**, p. 85.
[24] J. R. Nicholls, N. J. Simms, A. Encinas-Oropesa, *Mater. High Temp.* **2007**, *24*, 149.
[25] N. Birks, G. H. Meier, F. S. Pettit, *High-Temperature Oxidation of Metals*, Cambridge University Press, Cambridge **2006**.
[26] D. Young, *High Temperature Oxidation and Corrosion of Metals*, Elsevier, London **2008**.
[27] J. R. Nicholls, P. Hancock, *Analysis of Oxidation and Hot Corrosion Data—A Statistical Approach*, NACE, San Diego, CA **1983**,
[28] F. Pettit, *Oxid. Met.* **2011**, *76*, 1.

(Received: February 8, 2013) W7063
(Accepted: March 1, 2013)